Tectonophysics 686 (2016) 51–62

Contents lists available at ScienceDirect

Tectonophysics

journal homepage: www.elsevier.com/locate/tecto

Thermo-rheological aspects of crustal evolution during continental breakup and melt intrusion: The Main Ethiopian Rift, East Africa

Alessio Lavecchia [a,b,*], Fred Beekman [b], Stuart R. Clark [a], Sierd A.P.L. Cloetingh [b]

[a] Simula Research Laboratory, Fornebu, Norway
[b] Department of Earth Sciences, Utrecht University, Utrecht, the Netherlands

ARTICLE INFO

Article history:
Received 15 February 2016
Received in revised form 17 June 2016
Accepted 21 July 2016
Available online 25 July 2016

Keywords:
Main Ethiopian Rift
Temperature
Rheology
Metamorphism
Anatexis

ABSTRACT

The Cenozoic-Quaternary Main Ethiopian Rift (MER) is characterized by extended magmatic activity. Although magmatism has been recognized as a key element in the process of continental breakup, the interaction between melts and intruded lithosphere is still poorly understood. We have performed a 2D thermo-rheological modeling study of continental crust incorporating rheological variations due to melt intrusion-related thermal perturbation. The model is calibrated based on the characteristics of lithologies occurring in the MER and its extensional history, and includes the effect of metamorphism and anatexis on crustal strength and rheological features. During Miocene early rift phases strain in the MER was mainly accommodated through rift border faults, whereas Pliocene-to-recent extension history is characterized by magma assisted rifting with most strain accommodated across magmatic segments in the rift axis. Consequently, very little strain is distributed in the old Pan-African to Paleogene crust during Pliocene to Holocene times. The magmatic activity along the rift axis created ≈20 km thick magmatic segments, with growth rate estimated to range from ≈3.5 mm yr^{-1} to ≈6 mm yr^{-1}. Our model suggests that the strain transfer from Miocene rift border faults to magmatic segments was favored by a moderate increase in crustal strength, due to prograde metamorphism subsequent to the melt-induced thermal perturbation. Under such conditions, crustal stretching may not constitute an effective extension mechanism, thus strain may be preferentially accommodated by melt injection along hot, partially molten magmatic segments. Anatexis has been detected in our simulations, with melt fractions sufficient to break-up the crust solid framework and migrate. This determines local variations of rheological behavior and may induce seismicity. However, resulting melt percentages are not sufficient to induce widespread, crust-derived volcanic activity. Subsequently, volcanism in the MER is mainly due to mantle-derived melts, subjected to a various degree of fractionation, with minimal contribution from crust-derived magmas.

1. Introduction

Continental break-up is an important geodynamic process occurring during plate evolution, and may mark the response of the lithosphere when it is subject to tensional stresses of a sufficient intensity and duration. Plate rupture is the final result of the thinning and heating of the lithosphere, and is associated with upwelling of mantle material, whose decompression may lead to partial melting and subsequent magmatic activity (e.g. Ebinger and Sleep, 1998; Burov et al., 2007). This process is further enhanced when the mantle is subjected to thermal anomalies, such as in hot spot areas, where the presence of mantle plumes may also lead to lithosphere doming and extension (e.g. Burov et al., 2007; Burov and Gerya, 2014). The nature of the interaction between lithosphere- and plume-related tensile stress fields is subject to extensive debate, and their effective role in causing continental thinning and rupture (e.g. Burov et al., 2007, and references therein; Cloetingh et al., 2013). However, it is well established that mantle upwelling-related magmatic activity strongly favors plate extension and breakup (e.g. Buck, 2004, 2006). This is testified to by the collocation of extension and strong magmatic activity in many different areas, including a large number of passive continental margins worldwide. In such magmatic margins, thick sequences of igneous rocks may extrude, intrude and underplate the crust (e.g. Menzies et al., 2002). In many extensional models (e.g. Buck, 1991; Davis and Kusznir, 2004), magmatism is either absent or mainly considered as a consequence of rifting. This is in contrast with observations in extensional areas, where time relationships between igneous rocks emplacement ages and extension evolution demonstrate that magmatic activity occurs prior to, or simultaneously with, extension (e.g. Buck, 2006, and references therein). In addition, magmatic activity and rifting associated deformation may focus along inherited lithospheric heterogeneities (such as former suture zones), where the plume had the function of further triggering the rupture,

* Corresponding author at: Simula Research Laboratory, P.O. Box 134, 1325 Lysaker, Norway.
E-mail address: alessio@simula.no (A. Lavecchia).

http://dx.doi.org/10.1016/j.tecto.2016.07.018
0040-1951/

more than being the direct cause of rifting (e.g. Cloetingh et al., 2013; Buiter and Torsvik, 2014).

The presence of lithospheric heterogeneities may influence the extensional history of rifting areas. However, the evolution of plate strength and rheology, due to melt intrusion, is still poorly understood (e.g. Lavecchia et al., 2016). One of the least investigated aspects is the lithological evolution of rifting areas and their fertility (i.e. their capacity to produce melts when subjected to temperature and pressure variation). Although most magmatic products associated with rift areas are represented by mantle-derived melts, the presence of magmas characterized by a mixed (e.g. Thompson et al., 2001) or crustal origin (e.g. Kirstein et al., 2000) has been widely recognized. This testifies the profound effect that pressure and temperature conditions may exert on the same nature of the lithosphere, and, especially, on the crust.

One of the best studied rifting areas is the Main Ethiopian Rift (MER) (Fig. 1), a slowly extending continental rift constituting the northernmost section of the East African Rift System (e.g. Ebinger and Casey, 2001). Indeed, the relationship between magmatic activity, anomalous topographic swells and the presence of mantle plumes has long been recognized in the MER region (e.g. Ebinger and Sleep, 1998). However, both the evolution of the intruded crust and its response to the thermal perturbation are still poorly understood. These two elements are of a particular importance as the mantle lithosphere in this region is characterized by a marked thinning beneath the whole area (e.g. Ebinger and Sleep, 1998; Dugda et al., 2007), suggesting a major role of crust rheology in determining the strength of the whole plate.

In this paper, we present a thermo-mechanical model with the aim to examine the rheology variations of a continental crust subjected to a melt intrusion-related thermal perturbation. Our model includes temperature-induced metamorphic variations in crustal mineralogical association. The model characteristics have been calibrated adopting MER lithological and geometrical constraints, with the aim to better understand the evolution of the Ethiopian continental crust during the development of magma segments characterizing the axial rifting area.

2. Tectonic setting

The Main Ethiopian Rift (MER) (Fig. 1) constitutes the northern part of the East African Rift System (e.g. Ebinger and Casey, 2001) and converges, together with the Red Sea and Gulf of Aden rifts, in the Afar area. Among the three branches, it is the youngest and least evolved (e.g. Bastow et al., 2011, and references therein). The onset of extension in the MER is dated at ≈11–10 Ma (e.g. Ukstins et al., 2002; Wolfenden et al., 2004) within the Precambrian metamorphic crustal basement of the Pan-African Mozambique belt (Kazmin et al., 1978) and was mostly accommodated along mid-Miocene border faults delineating half-grabens (Morley, 1988; Wolfenden et al., 2004). The last phases of extension are characterized by an intense magmatic activity, leading to the construction of approximately 20 km thick, right-stepping, en echelon magmatic segments during the Pliocene-Pleistocene time (Ebinger and Casey, 2001; Beutel et al., 2010, and references therein; Bastow et al., 2011).

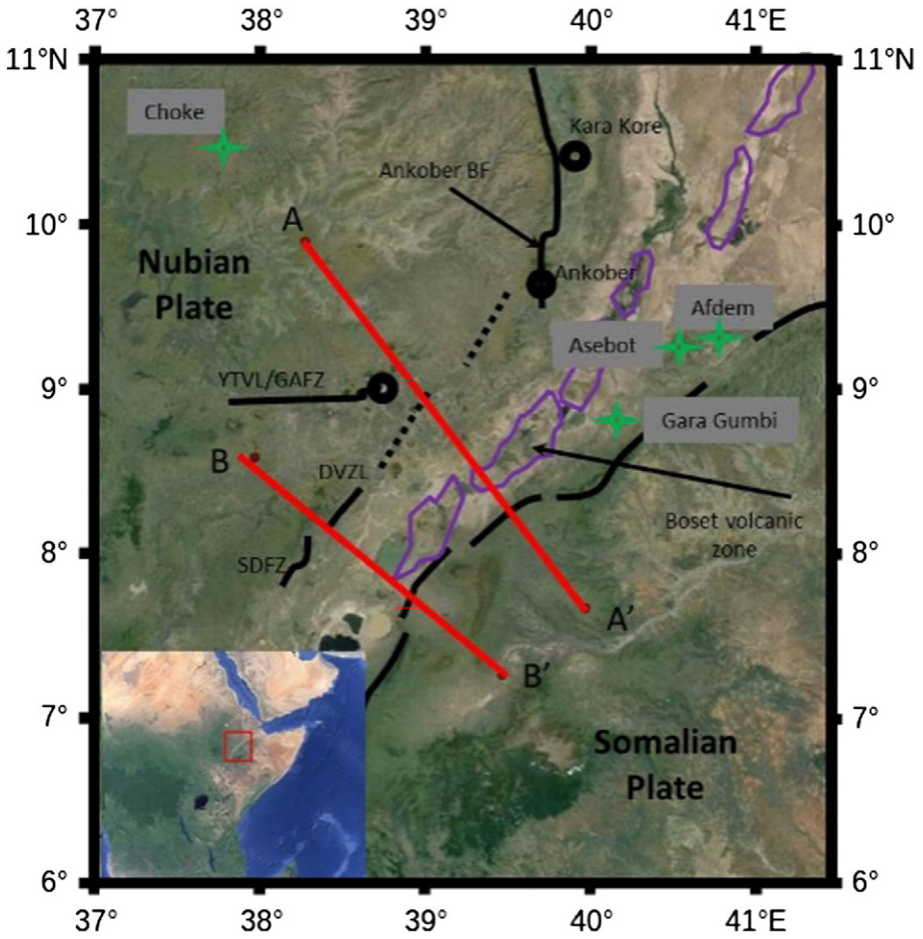

Fig. 1. Sketch map of Afar Rift and northern Main Ethiopian Rift (after Bastow et al., 2011, modified). Violet closed lines represent magmatic segments and solid black lines depict major mid-Miocene border faults. Dashed lines are faulted monoclines. Green stars are selected Cenozoic volcanoes. Red lines are the traces of gravimetric cross sections adopted for simulations (AA″: Cornwell et al., 2006; BB′: Mahatsente et al., 1999; see Fig. 2). SDFZ—Silti Debre Zeyit fault zone; GAFZ—Guder Ambo fault zone; YTVL—Yerer-Tullu Wellel volcanotectonic lineament. BF—Border Fault; DZVL—Debre Zeit Volcanic Lineament.

The strain pattern highlighted by geodetic and seismic studies shows that at present day the border faults are relatively inactive, with earthquakes concentrated within magmatic segments (e.g. Keir et al., 2006). The Main Ethiopian Rift is characterized by a seismic moment release in the MER that is <50% than what is expected from the estimated extension velocity (Hofstetter and Beyth, 2003), which suggests that most extension is accommodated aseismically. These observations are supported by gravity (Cornwell et al., 2006) and geodetic data (e.g. Ebinger and Casey, 2001), showing that >80% strain is accommodated along magmatic segments and without a marked crustal thinning. P- and S-wave tomography models indicate that the lithosphere–asthenosphere boundary lies at a depth of approximately 70 km, associated with the presence of a broad mantle upwelling beneath the MER and the Ethiopian plateau. The asthenosphere is characterized by some of the lowest-velocity worldwide (Bastow et al., 2011, and references therein) and constitutes the main source zone for melts emplaced in the MER and magma-assisted extension (e.g. Bastow et al., 2011). Deeper in the mantle, the low-velocity anomaly continues down to the transition zone, and likely connects to the African Superplume (Bastow et al., 2011). SKS analysis and crustal splitting observations point out that melt accumulates in vertically oriented dykes cross-cutting the lithosphere (e.g. Keir et al., 2005). Furthermore, magnetotelluric surveys highlight the presence of intruded and partially molten material; these melt zones occur at various depth in the crust and are associated with seismicity (Bastow et al., 2011).

Geophysical and geochemical data show that the crust has been extensively modified by magmatic modification and that the presence of melt is strictly related to extension by faulting. Crustal thickness is greatest (40–50 km) beneath the uplifted plateau flanking the rift valley, where thickness registered is approximately 45 km and associated with evidences of magmatic underplating (Dugda et al., 2005). Beneath the MER, crustal thickness decreases to values ranging from 38 km to 27 km, and are associated to Poisson's ratio values of 0.27 to 0.35, indicating a marked crustal thinning associated with massive presence of intruded mafic material and a presence of partial melting (Dugda et al., 2005) (Fig. 3).

3. Model description

3.1. Geometrical features

We used a 2D thermal model that numerically simulates the temperature variations in a multilayered crustal section, induced by the emplacement of a sequence of basaltic dykes, over a time span ranging from 1.6 Myr (Ebinger and Casey, 2001) to 3.0 Myr (Beutel et al., 2010, and references therein). The geometries and densities adopted in the model are based on previous reconstructions, based on works by Mahatsente et al. (1999) and Cornwell et al. (2006) (Fig. 2); they comprise a 35 km thick crust with a lateral extension of 40 km, divided in intervals with different density and mineralogical composition. The lateral crustal extension in the model ensures that the thermal perturbation does not propagate sufficiently fast to reach the crust boundary and create undesired overheating effects. The thermal loading is implemented by "injecting" a sequence of 400 dykes (conform Lavecchia et al., 2016), each being 25 m thick, forming a basaltic body growing by outward lateral accretion (from the right leftward). The magmatic segment growth rate corresponds to an intrusion rate ranging from ≈ 3.5 to ≈ 6 mm yr^{-1}.

The geometry implemented in the first case study (CR case study, Fig. 2a, b) incorporates the 2D density model obtained by Cornwell

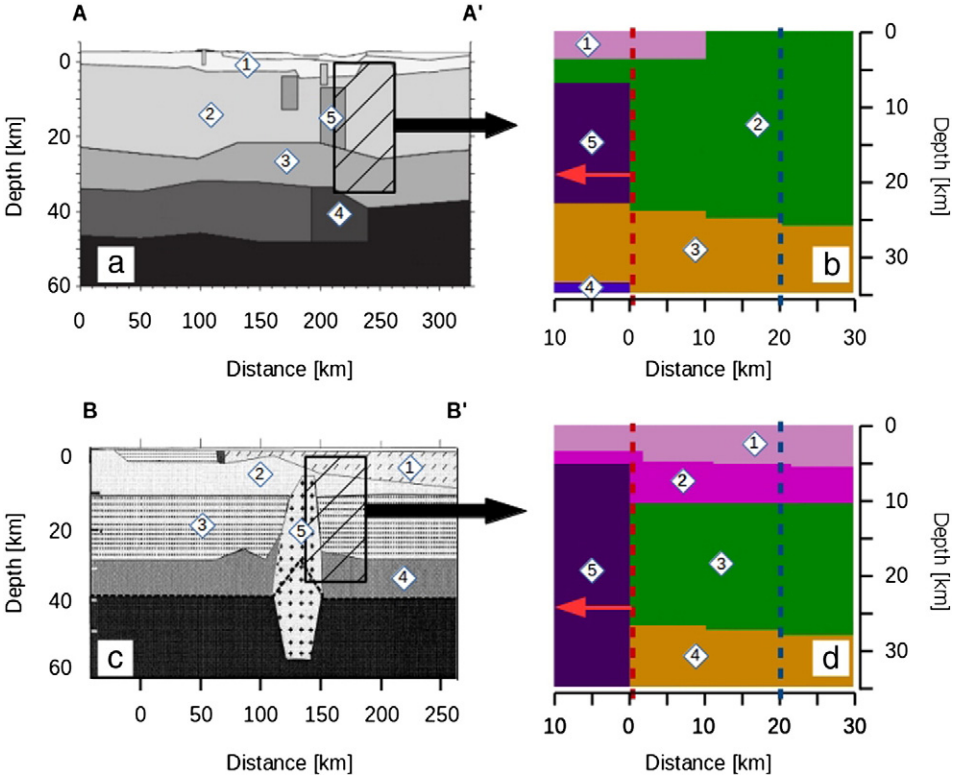

Fig. 2. Two vertical cross-sections of the northern MER, based on studies by Cornwell et al., 2006 (a, section AA′) and Mahatsente et al., 1999 (c, section BB′), and their geometrical representations adopted in the model (b, d). For location of the sections, see Fig. 1. The numbering refers to different layers inferred from constrains by geophysical studies (see text for explanation); red arrows point out the direction of the magmatic segment growth, indicating that each dyke is added to the previous segment by leftward lateral accretion. The red and blue dashed lines are the traces for differential stress-depth profiles (see Figs. 7, 8).

et al. (2006), where 5 main different bodies are detected at a depth < = 35 km:

1. A supra-basement interval, with density = 2570 kg m^{-3}, interpreted as pre-rift Jurassic to Palaeogene sedimentary rocks, interbedded with Oligocene flood basalts. The model takes into account the buried horst, constituting a rift flank related to the Arboye border fault (Cornwell et al., 2006, and reference therein);
2. An upper crust whose age ranges from lower to middle Proterozoic, composed of clastic metasediments;
3. A high density lower crust layer, interpreted as an Archean cratonic basement (age ≥ 2.5 Ga), composed of high grade gneisses (granulite to amphibolite facies) (Kazmin et al., 1978, and references therein), underplated by Oligocene and more recent material (Mackenzie et al., 2005).
4. A mafic wedge, interpreted as low density mantle (rather than high density underplate) and consistent with the presence of 3–5% partial melt (Cornwell et al., 2006, and reference therein).
5. A gabbroic body, intruded in correspondence of the rift axis, whose high conductivity suggests the presence of melts at present day (Cornwell et al., 2006, and references therein).

The second case study (MR case study, Fig. 2c, d) implements the geometry obtained by Mahatsente et al. (1999), where the following intervals are detected in the northern MER:

1. A cover interval, mainly constituted by siliceous domes and flows, whose composition ranges from pantellerites to obsidians to volcanoes characterized by andesite to rhyolite activity (Mahatsente et al., 1999).
2. An upper layer, interpreted as the upper part of the crystalline basement and correspondent to the Miocene Magdala group (Molly, 1959, and references therein); it is mainly constituted by rhyolites, trachytes, ignimbrites and basalts (Mahatsente et al., 1999).
3. An intermediate interval, whose density roughly corresponds with the clastic layer occurring in Bastow et al. (2011), and thus interpreted as such in our simulation.
4. A lower crust, with a lower density than the one adopted in the model by Bastow et al. (2011). We assume in our simulation that the difference in density is due to a lower volume of underplated material.
5. An intruded gabbroic body, whose density variation has been interpreted as due to difference in crust contamination in the upper portion by Mahatsente et al. (1999) (in our model we assign the same density for the whole body).

3.2. Thermal and petrogenetic features

The thermal evolution of the model is governed by the heat transfer Eq. (1):

$$\rho C_p \frac{\partial T}{\partial t} = k(T)\nabla^2 T + Q \quad (1)$$

where ρ is the density, C_p is the specific heat, T is the temperature, t is the time, k is the thermal conductivity and Q the internal heat production. The dyke emplacement has been assumed a quasi-instantaneous process, and hence the model does not take into account any advection of heat. The numerical solution is obtained by using FEniCS (Logg et al., 2012), a collection of free scientific computing codes for finite element based automated solution of partial differential equations.

The values adopted for different parameters are given in Table 1. We consider two different geotherms, both constituted by a temperature-dependent thermal conductivity, a fixed surface temperature of 25 °C a heat flux at the base of the crust of 27 mW m^{-2} and a heat flux at the lateral boundaries equal to 0. The different geotherms are distinguished in a "cold" geotherm, characterized by a transient temperature of 600 °C at the crust base, a "warm" geotherm, characterized by a temperature of 750 °C at the crust base. These different temperature values were chosen in order to compare different preliminary situations, where in the "cold" simulations we isolate the effect of thermal perturbation in an initially unperturbed continental crust, and in a "warm" case we take into account the possibility of a thermal perturbation (e.g. due to magmatic underplating) prior to dyke intrusion.

Table 1
Thermal and compositional parameters adopted in the model.

Parameter	Symbol and equation	Value
Surface temperature	T_s	25 °C
Crust base temperature	T_b	600 °C, 750 °C
Melt emplacement temperature	T_m	1300 °C
Melt solidus temperature	T_c	1100 °C
Model base heat flux	q_b	27 mW m^{-2}
Latent heat of crystallization	LH	400 kJ kg^{-1}
Radiogenic heat generation	$A(z) = A_0\exp(-z/D)$	$A_0 = 2$ μW m^{-3} $D = 12$ km

Case study and layer	Mineralogical assemblage [vol.%]	Density [kg m^{-3}]	A [W m^{-1} °C^{-1}]; B [W m^{-1}]
CR			
1	qz40, pl25, kfs35	2570	0.64; 807
2	chl30, ms25, qz25, pl10, kfs10	2790	0.75; 705
3	ms10, qz20, pl15, ky5, grt10, bt25, st5, kfs10	2940	0.75; 705
4	ol100	3230	0.73; 1293
5	ol100	3000	1.18; 474
MR			
1	qz40, pl25, kfs35	2500	0.64; 807
2	qz25, pl15, kfs45,	2700	0.64; 807
3	chl30, ms25, qz25, pl10, kfs10	2780	0.75; 705
4	ms10, qz20, pl15, ky5, grt10, bt25, st5, kfs10	2900	0.75; 705
5	ol100	3050	1.18; 474

LH value comes from Spear (1993); densities for different layers have been taken from Cornwell et al. (2006) and Mahatsente et al. (1999) (see text for further explanation). *A* and *B* parameters are used to calculate the temperature-dependent thermal conductivity, according to the formula: $k(T) = A + B / (350 + T\,[°C])$ (Clauser and Huenges, 1995, and references therein). Mineral abbreviations are as follows: bt = biotite, chl = chlorite, grt = garnet, kfs = K-feldspars, ky = kyanite, ms = muscovite, ol = olivine, pl = plagioclase, qz = quartz, st = staurolite.

The release of heat during melt crystallization in the dyke body has been taken into account for the cooling magma by implementing an effective specific heat instead of the true specific heat, in a temperature interval between 1300 and 1100 °C (Paterson et al., 1998, and references therein). The effective specific heat has been calculated on the basis of the formula by Spear (1993) (Ayalew and Gibson, 2009):

$$C_{eff} = C_p + \frac{LH}{\Delta T} \quad (2)$$

where C_{eff} is the effective specific heat, C_p is the specific heat, LH is the latent heat of crystallization and ΔT is the crystallization temperature interval.

Our model takes into account prograde metamorphism occurring in a polymineralic crust, including the most common minerals in crustal rocks (i.e. quartz, plagioclase, K-feldspars, allumosilicates, chlorite, muscovite, biotite, garnet, staurolite, olivine and water) (Table 1).

The metamorphic grid is illustrated in Fig. 3; the reaction stoichiometry has been calculated on the basis of oxides balance and kept fixed at different T-P conditions; it is as follows:

1) Ky-And-Sil
2) 3Chl + Ms. + 3Qz = Bt + 4Grt + 12Wt
3) 15Chl + 15Grt + 33Ms = 33Bt + 34Qz + 7St + 46Wt
4) 4Bt + 7Qz + St = 5Grt + 4Ms + 2Wt
5) Ms. + 5Qz + 2St = 18Als + Bt + Grt + 4Wt
6) 18Ab + 5Kfs + 50Qz + 26Wt = L
7) 13Ab + 18Ms + 47Qz + 70Wt = 14Als + 4Kfs + L
8) 13Ab + 11Als + 13Bt + 47Qz + 31Wt = 9Grt + 4Kfs + L.

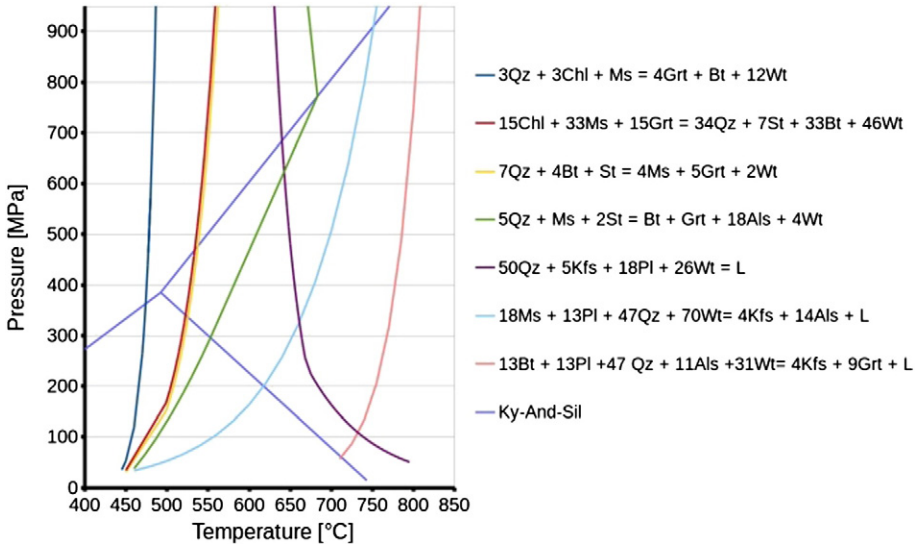

Fig. 3. Reaction grid used to simulate metamorphism in the crust. Reactions in the legend occur with increasing temperature. For mineral abbreviations see caption of Fig. 2. Additional abbreviations: als = allumosilicates; ky-and-sil = kyanite-andalusite-sillimanite; L = melt; wt = water.

The temperature-pressure curves have been extrapolated by Spear and Cheney (1989), while the curve for rhyolite melt generation (reaction 6) takes into account results by Luth et al. (1964) and the muscovite- and biotite-dehydration reactions (7 and 8) are calibrated on the basis of studies by Vielzeuf and Holloway (1988) and Patiño Douce and Johnston (1991).

In order to estimate the release/adsorption of heat during metamorphism, we have included the metamorphism-related reaction enthalpy in the thermal balance; this term has been quantified basing on the procedure described in Philpotts and Ague (2009).

In order to estimate the release/adsorption of heat during metamorphism, the enthalpy variation relative to each metamorphic reaction has been calculated, according to formula (3):

$$H = E + PV \tag{3}$$

where H is the enthalpy of the system, E is the internal energy, P is the pressure and V is the volume. For each mineral, the enthalpy of formation has been calculated according to Philpotts and Ague (2009) (Bergantz, 1989):

$$\Delta H = H_T^0 - H_{298}^0 = a(T-298) + \frac{b}{2}\left(T^2-298^2\right) - c\left(T^{-1}-298^{-1}\right) + 2d\left(T^{0.5}-298^{0.5}\right) \tag{4}$$

where H_T^0 is the mineral enthalpy of formation at standard pressure and given temperature, and H_{298}^0 is the mineral enthalpy of formation at standard pressure and temperature. a, b, c and d are thermodynamic parameters with values given by Holland and Powell (1998). Therefore, the reaction enthalpy is given by (Beutel et al., 2010):

$$\Delta H_{reaction} = \sum_{i=1}^{n} \Delta H_i - \sum_{j=1}^{m} \Delta H_j \tag{5}$$

where n and m are respectively the number of the products and the reactants in the metamorphic reaction.

3.3. Rheological features

Temperature estimations and calculated lithologies were used to calculate differential stress values σ (i.e. $\sigma = \sigma_1 - \sigma_3$) and to estimate the rheological behavior in the modeled crust by adopting the frictional criterion for the brittle field and the power-law creep equation for the ductile field (as described hereafter). We assume that the stress distribution in the crust is locally dominated by the rheological behavior requiring the lowest differential stress to activate, which for a multilayered crust results in a typical "Christmas tree" depth-dependent variation of differential stress with depth (e.g. Cloetingh et al., 2013). The adopted parameters are given in Table 2.

For the frictional criterion we have used the equation (Sibson, 1974) (Bialas et al., 2010):

$$\sigma_b = \sigma_1 - \sigma_3 = \beta \rho g z (1-\lambda) \tag{6}$$

where $\sigma_b = \sigma_1 - \sigma_3$ is the friction-related differential stress (compression is positive), β is a dimensionless parameter depending on the frictional coefficient and deformational regime, ρ is the rock density at depth z, g is gravity acceleration.

The flow law implemented in the model is (e.g. Ranalli, 1995; Gerya, 2010) (Boccaletti et al., 1995):

$$\dot{\epsilon} = A h^m (\sigma_d)^n \exp\left(\frac{-E + V_a P}{RT}\right) \tag{7}$$

where $\dot{\epsilon}$ is the strain rate, h is the grain size, raised to the power of the parameter m, σ_d is the differential stress (similarly to σ_b), P is the pressure, R is the gas constant, T is the temperature and A, n, E and V_a are minerals rheological parameters. Ductile deformation in the crust mainly occurs

Table 2
Rheological parameters adopted for minerals in the model.

Model mineral	Abbreviation	A [MPa^{-n} s^{-1}]	n	E [kJ mol^{-1}]
Chlorite	chl	1.1E−15	18	51[a]
Muscovite	ms	1.1E−15	18	51[a]
Biotite	bt	1.1E−15	18	51[a]
Quartz	qt	1.1E−4	4	223[b]
Plagioclase	pl	2.34E−6	3.9	234[c]
K-feldspar	kfs	2.34E−6	3.9	234[c]
Allumosilicates	als	23.4	4	410
Staurolite	st	23.4	4	410
Garnet	gt	276	3	444[d]

Parameters for staurolite and allumosilicates are the result of a mean between "weak" minerals (phyllosilicates, quartz and feldspars) and "strong" minerals (garnet) parameters, obtaining a fitting rheological behavior with a less deformable mineral than micas, quartz and feldspars, but still deformable and subject to recrystallization.

[a] Kronenberg et al. (1990).
[b] Gleason and Tullis (1995).
[c] Shelton and Tullis (1981).
[d] Wang and Ji (1999).

by dislocation creep, thus the term h^m assumes value 1 ($m = 0$), while the term V_aP has been neglected, being $V_aP \ll E$ (e.g. Ranalli, 1995).

The rheological parameters for the single minerals were used to calculate the parameters of the multiphase rock for each time-step, following the average procedure suggested by Ji et al. (2003, and references therein).

When rocks are partially molten, variations in both strength and rheology occur, according to the melt fraction generated during melt intrusion. Two thresholds have been considered in our model:

1. A first rheological threshold occurs with melt fraction $\Phi \approx 0.06$–0.08, corresponding to the Melt Connectivity Transition (MCT), and determines a breakup of the rock solid framework, with subsequent decrease in crust brittle strength, quantified as ≈ 1 magnitude order (e.g. Vanderhaeghe, 2001; Rosenberg and Handy, 2005).
2. A second rheological threshold occurs with melt fraction $\Phi \approx 0.3$ and corresponds to the Rheologically Critical Melt Percentage (RCMP) (Arzi, 1978). In a crystals-melt mush, this threshold marks the transition from a solid to a liquid system.

When melt fraction exceeds the RCMP, we have adopted the rheology of rocks involved as purely Newtonian, with a viscosity calculated by using the Arrhenius Eq. (8) (Dingwell, 1995):

$$\log_{10}(\eta_T) = \log_{10}(\eta_0) + 2.303\frac{E}{RT} \tag{8}$$

where η_T is the melt viscosity at temperature T, η_0 is a pre-exponential factor, E is the activation energy and R is the gas constant. Data for viscosity curve calibration are taken from Shaw (1965), relative to magmas with 4 vol.% H_2O, leading to values $\eta_0 = -3.0$ and $E = 36{,}500$.

4. Results

Two-dimensional model calculations have been carried out for simulation times of 1.6 Myr and 3.0 Myr, testing two different isotherms, characterized by a bottom temperature of, respectively, 600 °C and 750 °C. The monitored temperature variations are here shown as 2D isotherms contours (Figs. 4, 5), as partial melting sections (Fig. 6) and (σ_d,z) paths (Figs. 7, 8).

As shown by the isotherm trend in both the crustal geometries adopted (Figs. 4, 5), when the simulation time span Δt is 1.6 Myr the thermal perturbation due to melt emplacement affects the crust laterally for a distance of $\approx$15 km from the dyke intrusion. If the value of Δt is increased to 3 Myr, then the propagation distance of thermal perturbation slightly exceeds 20 km; at a depth > 20 km the crust undergoes significantly more heating in the MR case study than in the CR reconstruction, due to the different estimated sizes of the intruded body. At the same time at the top of the intruded body we observe smaller temperature differences and a slightly farther propagation of the thermal perturbation in the CR compared to the MR case study. These small variations at shallow depths are due both to the cooling effect at the surface and the temperature-dependent thermal conductivity; the latter is characterized by higher values in the CR model setting.

In the MR case study (Fig. 5), the temperature registered in the lateral dyke aureole shows negligible differences when we adopt different geotherms and keep the model geometry unvaried. However, the temperature shows a marked increase when shorter simulation times (and thus higher intrusion rates) are taken into account, denoting a primary control exerted by magma intrusion rates on the temperature field. In the CR reconstruction (Fig. 4), the effect of different adopted geotherms on the registered thermal perturbation is also marked laterally and at the bottom of the intruded dyke body, due to the smaller size of the magmatic segment. In our case, the different geotherms lead to temperature differences of up to 100 °C.

In the innermost part of the intruded body, we observe that registered temperatures exceed 1100 °C in all our simulations. This latter value has been chosen as our solidus temperature for basaltic melts (e.g. Paterson et al., 1998, and references therein), assuming in our simulations that fractioned crystallization does not determine appreciable variations in the melt solidus temperature. As already observed in the temperature field at the top of the dyke body, temperature variations are mostly influenced by the intrusion rates: in both the CR and MR case study, by considering a growth time of 1.6 Myr, we observe that the innermost interval of the intruded body is still molten at depth varying from 7.5 km to 9 km, whereas with a growth time of 3.0 Myr, temperatures are $\approx$200 °C lower in the same location.

By varying both the geometry and the geotherm in our model, we observe that the melt production affects extended intervals of the crust, with produced volumes $\approx$ 20–27 vol.% (Fig. 6). At shallow to mid depths, melt production closely follows the heat diffusion. As a consequence, a growth time of 3.0 Myr favors extended partial melting, compared with an intrusion duration of 1.6 Myr, due to the longer time available for heat propagation. Melt productivity drastically reduces in proximity of the boundary between upper and lower crust due to a decrease crust fertility. In addition, the lower crust comprises a deep basal layer where the volume of produced melt depends on the chosen geotherm. When the imposed temperature at the base of the crust is 600 °C, melt does not exceed 6 vol.% and is strictly coupled with propagating thermal perturbation from the dykes. On the other hand, a crust base temperature of 750 °C determines values $\approx$13 vol.%, affecting extensively the crustal base.

The variations in mineralogical assemblages due to temperature increase and subsequent metamorphism cause pronounced variations in crustal strength values and rheological behavior in space and time (Figs. 7, 8). In all the simulations carried out (Figs. 4, 5), we observe an increase in strength in the upper crust, which is coupled with the propagation of the thermal perturbation at temperatures between 500 °C and 600 °C. The metamorphic reactions included in our models determine an increase in volume percentage of minerals characterized by marked strength (mainly feldspars and garnet). This occurs at the expense of minerals characterized by low strength values, namely quartz and micas. The most notable strength increase is observed during the first 200 kyr after the intrusion onset, i.e. during early stages of crustal heating. This has been interpreted as an effect of the low temperature metamorphic reactions and, more specifically, as related to garnet appearance at relatively low temperatures, due to Mn presence. In addition, temperature increase is accompanied by crustal anatexis, which has a profound effect on both crust strength and rheology, especially when a "hot" geotherm is considered. The two combined effects cause a transition from ductile to brittle behavior in the most proximal areas to the sides, and partially above, the intruded body (Fig. 7).

In our models, the adopted geotherm determines important variations in the calculated differential stress values (σ) (Fig. 7). In all our simulations we observe the presence of a brittle layer characterized by relatively high σ values, and marking the upper-lower crust boundary. When a "cold" geotherm is adopted, this interval is located at a depth $\approx$ 27 km. In contrast, the adoption of a "hot" geotherm causes this layer to move up at a depth of <20. This causes an unexpected strength increase up to an order of magnitude, accompanied by a transition from a ductile to a brittle rheology at a depth between 20 km and 25 km, because the equilibrium of mineralogical associations is characterized by higher strength. The effect of melts on the rheological behavior is also predicted at the base of the crust where a $\approx$5 km thick brittle interval, coupled with a drop in σ values, has formed due to partial melting.

The magmatic segment aureole is the location where the interaction between melt production and rheology appears more evident (Fig. 8); in all our simulations the crust shows high strength values only in the uppermost layer ($\approx$4 km in the CR case study, to 10 km in the MR case study), and subsequently it is subjected to a marked drop in σ values. This decrease, however, is not accompanied by a switch from a brittle to a ductile rheological behavior. In contrast, brittle behavior is maintained up to depths of $\approx$25 km in both case studies. In the CR

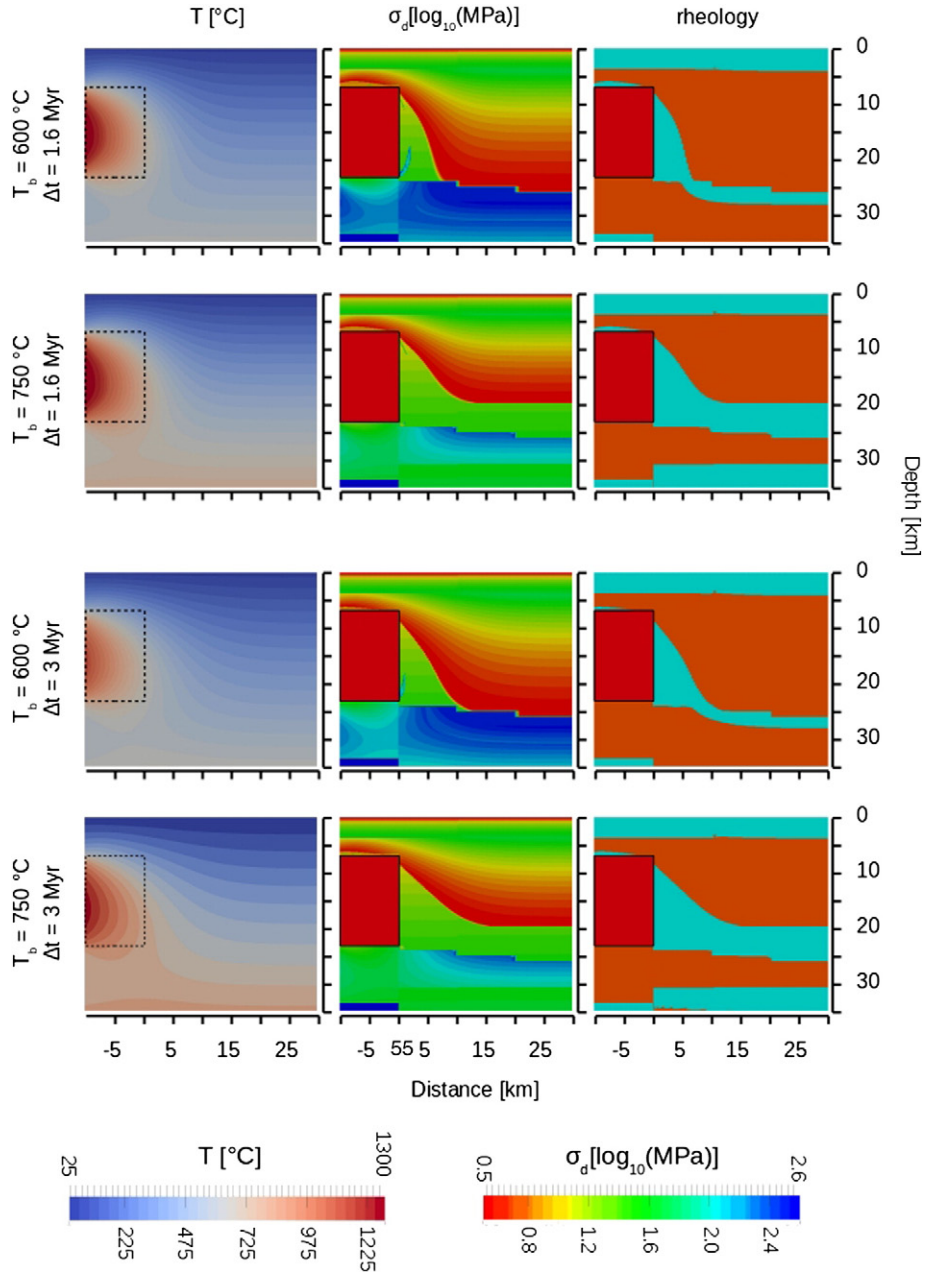

Fig. 4. Temperature (T, left column), differential stress (σ_d, center) and rheology contour sections (right) in the CR case study (see Figs. 1, 2, section AA′), at the end of the simulation. T_b indicates the temperature adopted at the base of the model. Δt indicates the time step represented in the figure, coincident with the end of the simulation and the complete growth of the magmatic segment (top panels, $\Delta t = 1.6$ Myr; bottom panels, $\Delta t = 3$ Myr). The light blue field in the brittle-ductile transition contour sections represents the brittle behavior, while the orange field represents the ductile behavior. The areas bounded by the black dashed lines in the left panels and the red boxes in the middle and right panels represent the geometry of the intruded dyke body.

reconstruction, the lower layers in the model are subjected to partial melting only when the temperature adopted at the base is 750 °C. Together with the relatively small dimension of the magmatic segment, this determines higher value of crustal strength and a brittle behavior of the aureole only when anatexis occurs. However, in the MR case study the base of the dyke aureole exhibits ductile behavior, although melt is still produced, leading to larger sizes of the magmatic segments and the high temperatures reached.

5. Discussion

Most previous studies relate the presence of axial mafic bodies in areas of crustal extension and breakup with an overall weakening of the intruded crust (e.g. Buck, 2004; Bialas et al., 2010). In this paper we propose that a thermal perturbation related to melt emplacement in a crust with a polymineralic lithology causes crustal strengthening. This behavior occurs only at a limited distance from the intruded body, causing an increase in strength of the rocks (Figs. 4, 5) where there is direct contact with generated melts.

At present day, the Main Ethiopian Rift is characterized by >80% strain accommodated along magmatic segments, without evidences of a marked crustal thinning. Thermo-rheological models where mineral assemblage is kept constant throughout the simulation shows that the emplacement of dykes is accompanied by crustal heating and, subsequently, progressive weakening. Under such conditions, magma-assisted crustal rifting by repeated dyke injection should also be accompanied by distributed strain across the weakened crust, thus hampering the marked localization of the extension in the MER along-axis

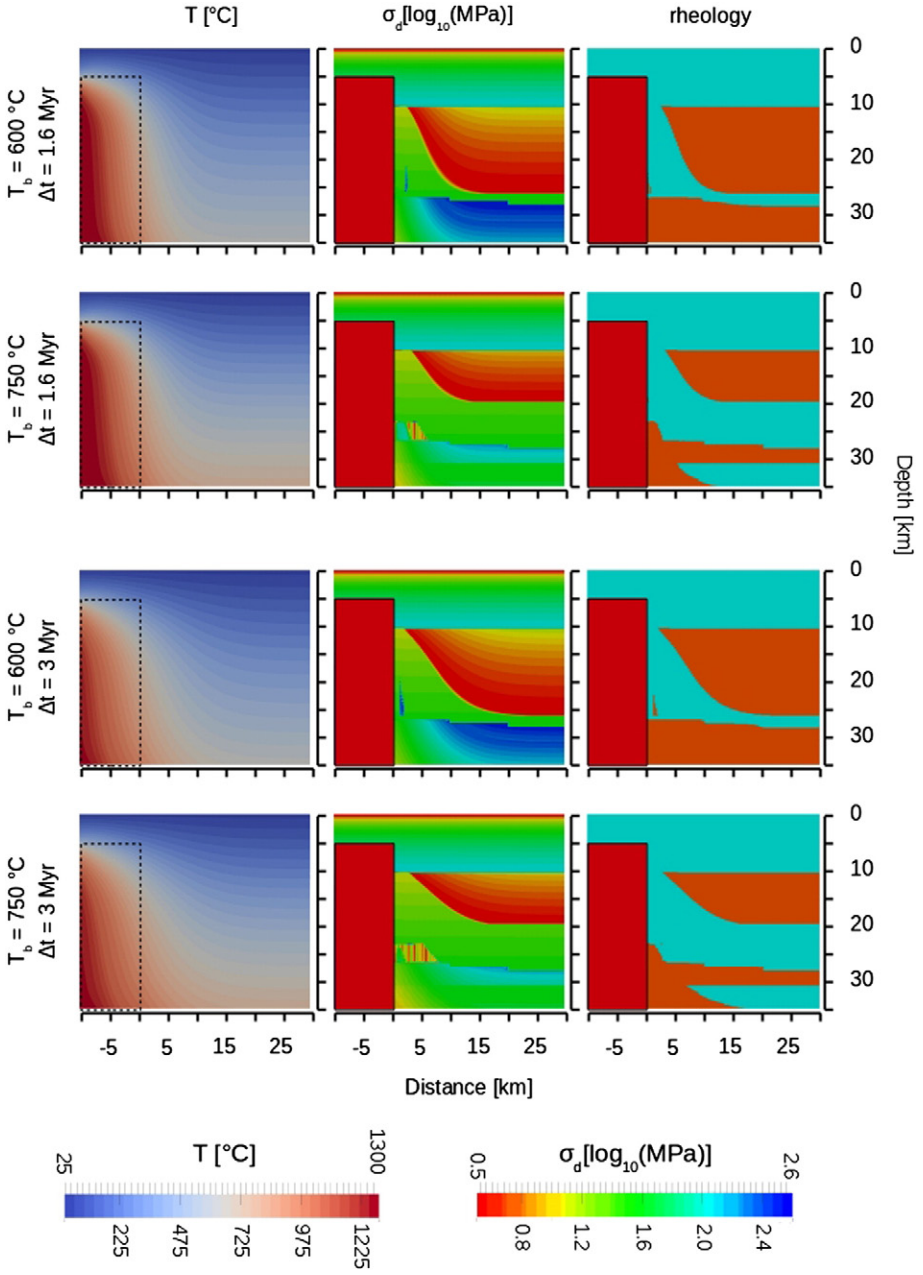

Fig. 5. Temperature (T, left column), differential stress (σ_d, center) and rheology contour sections (right) in the MR case study (see Figs. 1, 2, section BB′), at the end of the simulation. T_b indicates the temperature adopted at the base of the model. Δt indicates the time step represented in the figure, coincident with the end of the simulation and the complete growth of the magmatic segment (top panels, $\Delta t = 1.6$ Myr; bottom panels, $\Delta t = 3$ Myr). The light blue field in the brittle-ductile transition contour sections represents the brittle behavior, while the orange field represents the ductile behavior. The areas bounded by the black dashed lines in the left panels and the red boxes in the middle and right panels represent the geometry of the intruded dyke body.

magmatic segments. In addition, our model shows that dyke intrusion is accompanied also by a progressive, albeit moderate increase in crustal strength. This also may contribute to localization of the extension in the rift axial region by dyke filling, conform previous results (e.g. Buck, 2004, 2006).

At high intrusion rates, the internal part of the dyke body remains partially molten, and therefore it constitutes a weak crustal zone. Consequently, this interval is a favorable area for melt intrusion, contributing in localization of deformation in the axial rift zone, in line with results obtained by Beutel et al. (2010).

The increase of the differential stress values in the upper and middle aureole, following the emplacement of magmatic segments, is accompanied by a switch from ductile to brittle rheological behaviors (Fig. 8). This variation is mostly due to the formation of new mineral associations, but is also promoted by crustal anatexis. Consequently, stress may be initially localized in this interval and accompanied by the formation of cracks and vein networks. The presence of melts in the MER crust, intruded at various depth (Beutel et al., 2010), is widely observed by tomographic (e.g. Guidarelli et al., 2011), seismic (Keir et al., 2005) and magnetotelluric (Whaler and Hautot, 2006) studies, and is mainly characterized by both mafic sills and dykes (e.g. Bastow et al., 2011) and felsic products (e.g. Boccaletti et al., 1999).

At present day, seismic activity in the MER is mostly distributed along the rift axis at a depth < 15 km within a 20 km wide zone of Quaternary eruptive centers (Keir et al., 2006). In our reconstruction, the estimated depth of the brittle-ductile transition in the upper crust ranges from a depth of ≈5 km to ≈10 km, in agreement with previous studies (see Daniels et al., 2014, and references therein). However, our

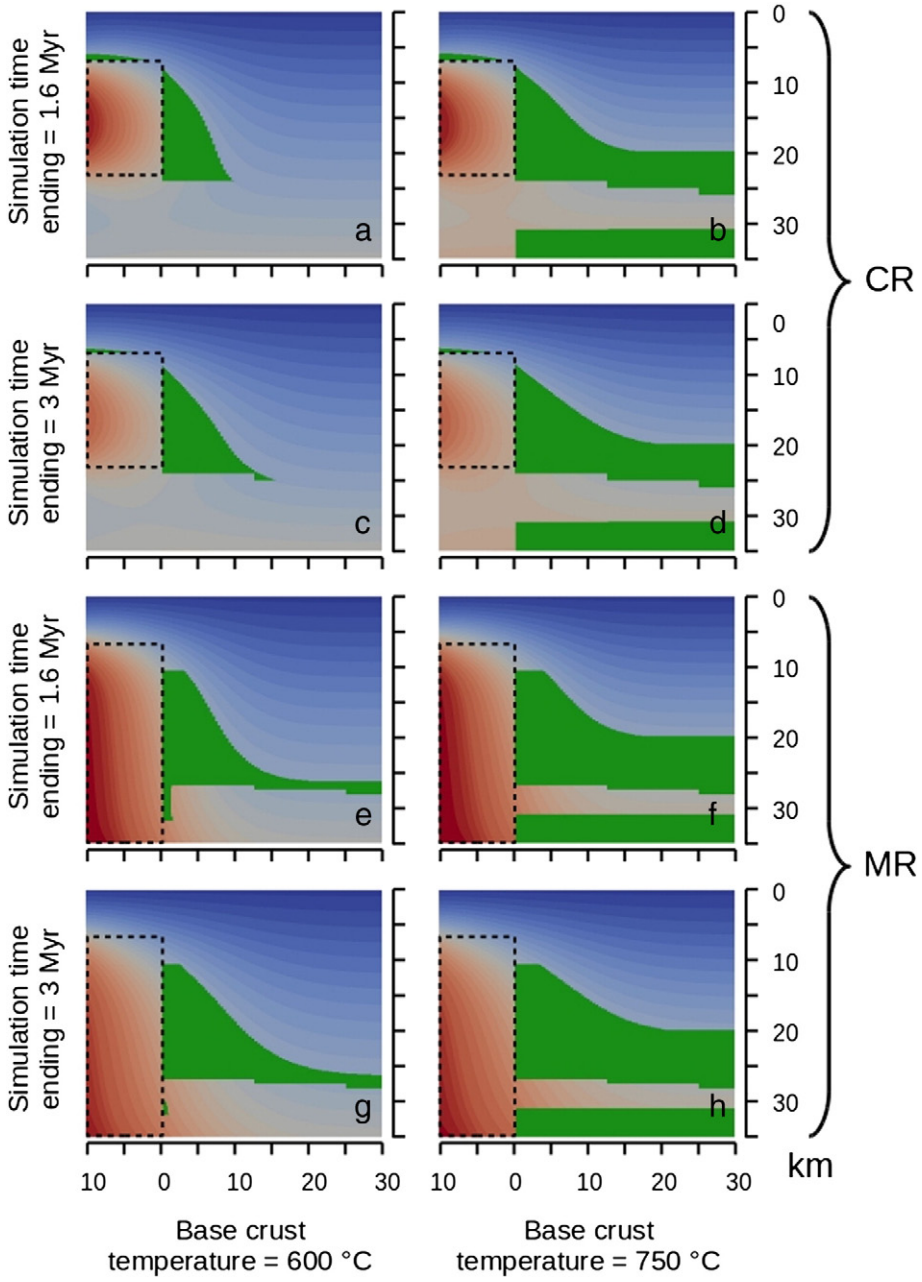

Fig. 6. Temperature sections for both the CR and the MR case studies. Green areas indicate where generated melt fraction leads to significant strength reduction and rheological variation. Left panels are for a geotherm where the temperature at the base of the crust is 600 °C, while right panels are for a geotherm where the temperature at the base of the crust is 750 °C. The areas bounded by the black dashed lines represent the geometry of the intruded dyke body.

observations suggest that melt production may exceed the MCT threshold even at shallow depths. Since the rock framework controls magma mobility (e.g. Vanderhaeghe, 2001) it appears that this depth, where melt migrates and where brittle behavior is enhanced by melts intrusion, may be locally underestimated. Consequently, we propose that the dyke aureole and the lower crust are favorable locations for anatexis, and that melt percentages are sufficiently high to cause break-up of the solid structure of the rocks, thus promoting further seismic activity.

According to Rooney et al. (2007) and Ayalew and Gibson (2009), volcanic activity in the MER does not show clear evidence of interaction between deep, plume-related melts and continental crust, but should be ascribed to fractionation of melts at various depths. At the same time, other studies show that Quaternary basalts are 10–13% contaminated by the lower crust (e.g. Boccaletti et al., 1995). Our results show that a "hot" geotherm, related to episodes of melt ponding and pre-dating the dyking event, may determine partial melting in the lower crust. On the other hand, when the base of the crust is characterized by cooler temperatures, melt injection is needed for crustal anatexis. The MER crust is characterized by crustal thicknesses ranging from 27 km to 38 km, and Poisson's ratio values ranging from 0.27 to 0.35. This indicates that MER crust has been extensively intruded by mafic rocks (Dugda et al., 2005), and consequently higher temperatures may be expected at its base. As a result, the presence of partial melts may be expected at the base of the lower crust. However, volcanic activity related to the presence of crust-derived magmas is expected only when the melt fraction reaches a threshold of 30% to 50% (Bergantz, 1989, and references therein). Such high melt fractions were not predicted in any of our simulations, and we, therefore, tend to exclude the possibility of a widespread volcanic activity of crustal origin.

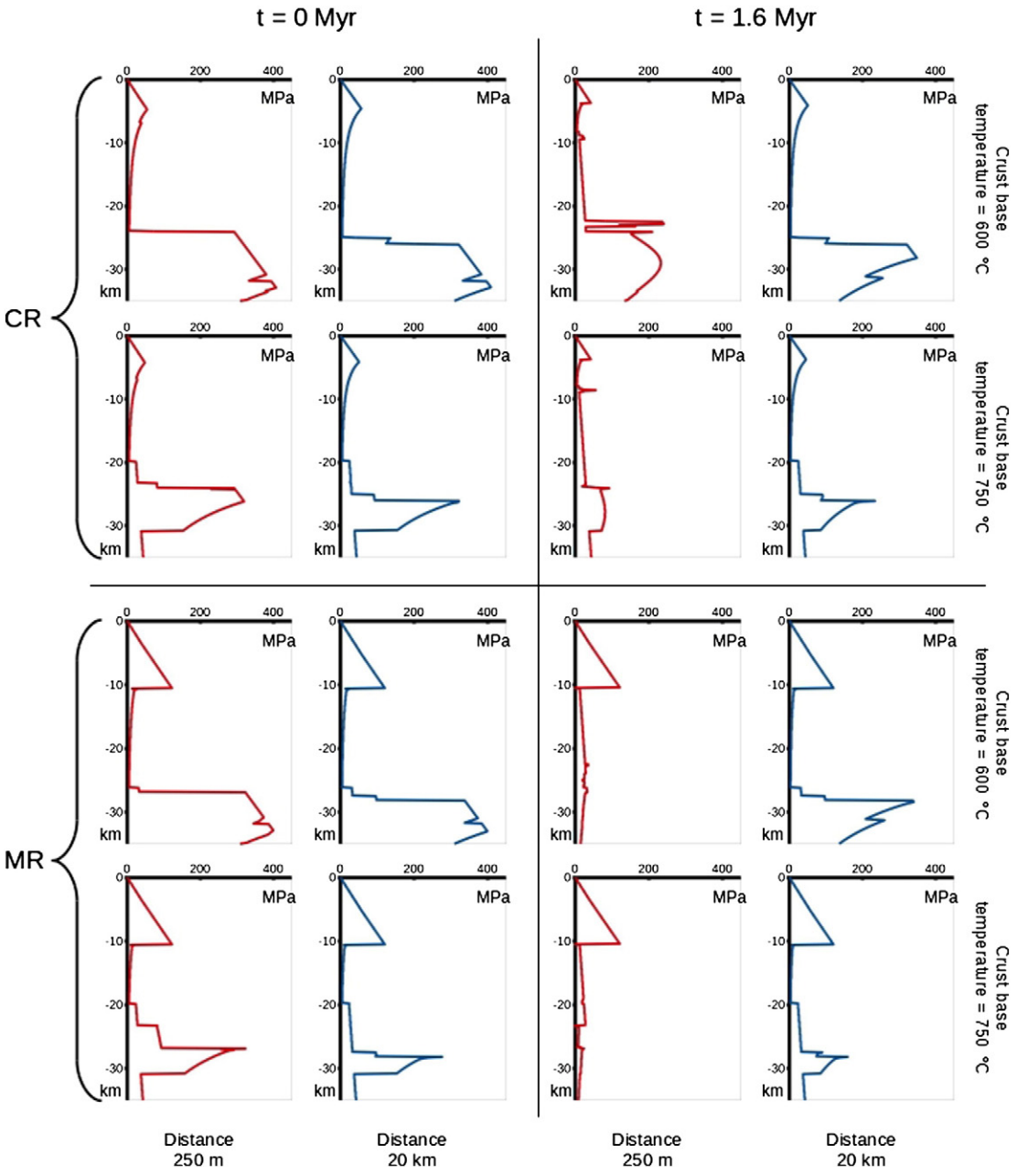

Fig. 7. Differential stress-depth diagrams for the CR and MR case studies, relative to a simulated time of 1.6 Myr. Left panels illustrate strength profiles in the crust prior to dyke intrusion, whereas values in the right panels correspond to the end of simulation. See Fig. 2 for locations of the profiles. Red profiles are located at a lateral distance of 250 m away from the intruded dykes (red lines, Fig. 2b, d), whereas the blue profiles are located at a distance of 20 km (blue lines, Fig. 2b, d). Horizontal axis scale is expressed in MPa; vertical axis scale is expressed in km. All the profiles relative to the thermally perturbed aureole show a moderate increase in differential stress values at a depth between 10 km and 25 km, despite the presence of a melt exceeding the MCT threshold.

Unlike findings by Corti (2008, 2009), who argued that the rift evolution and segmentation are independent of magmatic processes and controlled only by rift obliquity, our modeling results show that magmatic processes do play a key role in the Main Ethiopian Rift development. These two mechanisms, including mutual feedbacks, may significantly affect the thermo-mechanical structure of the Main Ethiopian Rift, resulting in the localization of deformation and magmatic activity along the rift axis.

Gravimetric studies by Cornwell et al. (2006) highlight the presence of a dense body at the top of the main dyke body located at the rift axis, situated beneath the Boset volcano at a depth between 2 km and 7.5 km. This body is characterized by a density of 2850 kg m^{-3} and is composed of <25% gabbroic material. Two hypotheses have been formulated for the origin of this intruded body: 1) fractionation of pre-emplaced melts, or 2) partial melting of crust and sediments due to previous intruded material. According to our model, temperatures at the roof of the dyke body may lead to partial melting of crustal material in a very thin layer above the magmatic segment. Furthermore, the recorded melt fraction is lower than the MCT threshold. As a consequence, the produced melt is devoid of mobility and not sufficient to justify the dimension of this felsic body. We therefore propose that the presence of the melt body is mostly due to fractionation of pre-intruded magmas at various depths in the crust, with a minimal contribution of crustal material.

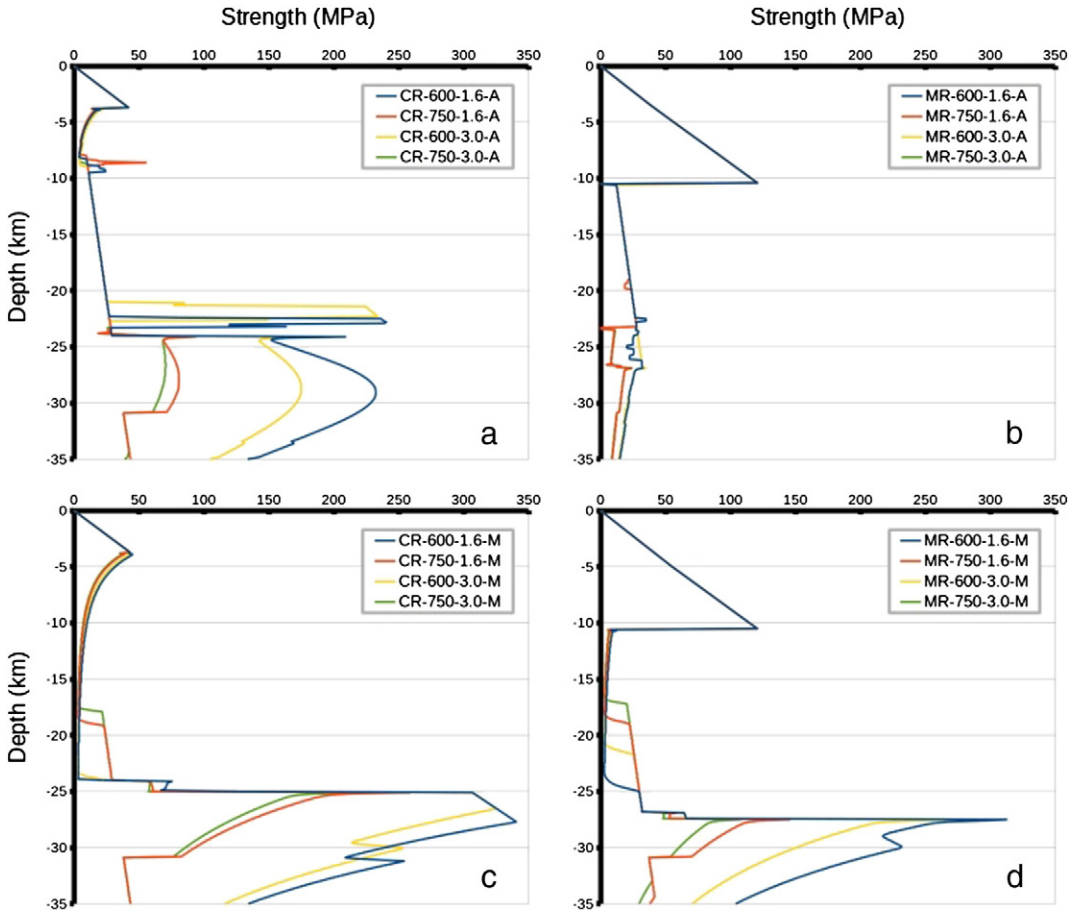

Fig. 8. Differential stress-depth profiles for the crust in the CR (left panels) and MR (right panels) case studies. Legend gives adopted temperature at the base of the model (°C) and total simulated time (Myr) for each case study. For the measurement location, see the red (panels a and b) and blue (c and d) dashed lines in Fig. 2. The CR case study is associated with an overall weakness of the upper crust, down to a depth of 20 km, followed by a pronounced differential stress increase. In the MR case study, strength is focused in the top 10 km.

6. Conclusions

We have investigated the effect of metamorphism and melt production on the crust of the Main Ethiopian Rift, resulting from the development of magmatic segments characterizing the axial zone of the rifting area. Our aim was to provide a more realistic description of the evolution of the MER crustal rheology and to better understand the interaction occurring between melts and intruded rocks in view of their effect on crustal strength.

For a polymineralic and metamorphism-sensitive crust an important predicted effect is the moderate increase in crustal strength in proximity of the magmatic segments, which increasingly affects larger volumes of crust when the thermal perturbation propagates into the crust. This behavior could explain the observed transition in the MER from initial rift phases, when strain is mostly accommodated by crust extension, to more recent Plio-Quaternary phases, when strain accommodation is mostly due to magmatic processes and is concentrated along axial intruded bodies in an estimated percentage > 80%.

The thermal perturbation due to the magma presence is accompanied by the production of crustal anatexis derived melts, which locally may migrate. The produced amount of melt is sufficient to induce variations in the depth of the brittle-ductile transition, and thus promote seismicity. At the same time, crustal anatexis can probably not feed widespread volcanic activity due to the relatively low melt production in the investigated area.

This study represents a first step in tracing the evolution of crustal scale features during continental rifting phases, especially when lithosphere breakup is accompanied by extended magmatic activity. Further research may focus on the effect of rheological stratifications in the MER, to better understand the influence of strain partitioning on the evolution of MER especially during initial rift phases.

Acknowledgements

This study has been funded by Simula School of Research and Innovation, P.O. Box 134, 1325 Lysaker, Norway, and the Netherlands Research Center for Integrated Solid Earth Science. The data for this paper are available by contacting the corresponding author. We thank Alexander Koptev for his thorough and constructive review.

References

Arzi, A., 1978. Critical phenomena in the rheology of partially melted rocks. Tectonophysics 44, 173–184.

Ayalew, D., Gibson, S.A., 2009. Head-to-tail transition of the Afar mantle plume: geochemical evidence from a Miocene bimodal basalt–rhyolite succession in the Ethiopian Large Igneous Province. Lithos 112, 461–476.

Bastow, I.D., Keir, D., Daly, E., 2011. The Ethiopia Afar Geoscientific Lithospheric Experiment (EAGLE): probing the transition from continental rifting to incipient seafloor spreading. In: Beccaluva, L., Bianchini, G., Wilson, M. (Eds.), Volcanism and Evolution of the African Lithosphere. Geol. Soc. of Am. Spec. Pap. 478, pp. 51–76. http://dx.doi.org/10.1130/2011.2478(04).

Bergantz, G.W., 1989. Underplating and partial melting: implications for melt generation and extraction. Science 245 (4922), 1093–1095.

Beutel, E., van Wijk, J., Ebinger, C., Keir, D., Agostini, A., 2010. Formation and stability of magmatic segments in the Main Ethiopian and Afar rifts. Earth Planet. Sci. Lett. 293, 225–235.

Bialas, R.W., Buck, W.R., Qin, R., 2010. How much magma is required to rift a continent? Earth Planet. Sci. Lett. 292, 68–78.

Boccaletti, M., Getaneh, A., Mazzuoli, R., Tortorici, L., Trua, T., 1995. Chemical variations in a bimodal magma system: the Plio-Quaternary volcanism in the Dera Nazret area (Main Ethiopian Rift, Ethiopia). Afr. Geosci. Rev. 2, 37–60.
Boccaletti, M., Mazzuoli, R., Bonini, M., Trua, T., Abebe, B., 1999. Plio-Quaternary volcanotectonic activity in the northern sector of the Main Ethiopian Rift: relationships with oblique rifting. J. Afr. Earth Sci. 29, 679–698.
Buck, W.R., 1991. Modes of continental lithospheric extension. J. Geophys. Res. 96, 20,161–20,178.
Buck, W.R., 2004. Consequences of asthenospheric variability on continental rifting. From. In: Karner, G.D., Taylor, B., Driscoll, N.W., Kohlstedt, D.L. (Eds.), Rheology and Deformation of the Lithosphere at Continental Margins. Columbia Univ. Press, pp. 1–31.
Buck, W.R., 2006. The role of magma in the development of the Afro-Arabian Rift System. In: Yirgu, G., Ebinger, C.J., Maguire, P.K.H. (Eds.), The Afar Volcanic Province Within the East African Rift System. Geol. Soc. Lond. Spec. Publ. 259, pp. 43–54.
Buiter, S.J.H., Torsvik, T.H., 2014. A review of Wilson Cycle plate margins: a role for mantle plumes in continental break-up along sutures? Gondwana Res. 26, 627–653.
Burov, E., Gerya, T., 2014. Asymmetric three-dimensional topography over mantle plumes. Nature 513, 85–89. http://dx.doi.org/10.1038/nature13703.
Burov, E., Guillou-Frottier, L., d'Acremont, E., Le Pourhiet, L., Cloetingh, S., 2007. Plume head–lithosphere interactions near intra-continental plate boundaries. Tectonophysics 434, 15–38. http://dx.doi.org/10.1016/j.tecto.2007.01.002.
Clauser, C., Huenges, E., 1995. Thermal conductivity of rocks and minerals. In: Ahrens, T.J. (Ed.), Rock Physics and Phase Relations. A Handbook of Physical Constants. AGU Reference Shelf 3. Am. Geophys. Union, Washington DC, pp. 105–126.
Cloetingh, S., Burov, E., Matenco, L., Beekman, F., Roure, F., Ziegler, P.A., 2013. The Moho in extensional tectonic settings: insights from thermo-mechanical models. Tectonophysics 609, 558–604.
Cornwell, D.G., Mackenzie, G.D., England, R.W., Maguire, P.K.H., Asfaw, L.M., Oluma, B., 2006. Northern Main Ethiopian Rift crustal structure from new high-precision gravity data. In: Yirgu, G., Ebinger, C.J., Maguire, P.K.H. (Eds.), The Afar Volcanic Province Within the East African Rift System. Geol. Soc. Lond. Spec. Publ. 259, pp. 307–321.
Corti, G., 2008. Control of rift obliquity on the evolution and segmentation of the main Ethiopian rift. Nat. Geosci. Lett. 1, 258–262. http://dx.doi.org/10.1038/ngeo160.
Corti, G., 2009. Continental rift evolution: from rift initiation to incipient break-up in the Main Ethiopian Rift, East Africa. Earth Sci. Rev. 96, 1–53.
Daniels, K.A., Bastow, I.D., Keir, D., Sparks, R.S.J., Menand, T., 2014. Thermal models of dyke intrusion during development of continent-ocean transition. Earth Planet. Sci. Lett. 385, 145–153.
Davis, M., Kusznir, N., 2004. Depth-dependent lithospheric stretching at rifted continental margins. In: Karner, G.D., Taylor, B., Driscoll, N.W., Kohlstedt, D.L. (Eds.), Rheology and Deformation of the Lithosphere at Continental Margins. Columbia Univ. Press, pp. 92–137.
Dingwell, D.B., 1995. Viscosity and anelasticity of melts. In: Ahrens, T.J. (Ed.), Mineral Physics and Crystallography. A Handbook of Physical Constants. AGU Reference Shelf 2. Am. Geophys. Union, Washington DC, pp. 209–217.
Dugda, M.T., Nyblade, A.A., Julia, J., Langston, C.A., Ammon, C.J., Simiyu, S., 2005. Crustal structure in Ethiopia and Kenya from receiver function analysis: implications for rift development in eastern Africa. J. Geophys. Res. 110, B01303. http://dx.doi.org/10.1029/2004JB003065.
Dugda, M.T., Nyblade, A.A., Julia, J., 2007. Thin lithosphere beneath the Ethiopian Plateau revealed by a joint inversion of Rayleigh wave group velocities and receiver functions. J. Geophys. Res. 112, b08305. http://dx.doi.org/10.1029/2006jb004918.
Ebinger, C.J., Casey, M., 2001. Continental breakup in magmatic provinces: an Ethiopian example. Geology 29, 527–530. http://dx.doi.org/10.1130/0091-7613(2001)029<0527:CBIMPA>2.0.CO;2.
Ebinger, C.J., Sleep, N.H., 1998. Cenozoic magmatism throughout east Africa resulting from impact of a single plume. Nature 395, 788–791.
Gerya, T., 2010. Introduction to Numerical Geodynamic Modelling. Camb. Univ. Press, UK, p. 345.
Gleason, G.C., Tullis, J., 1995. A flow law for dislocation creep of quartz aggregates determined with the molten salt cell. Tectonophysics 247, 1–23.
Guidarelli, M., Stuart, G., Hammond, J.O.S., Kendall, J.M., Ayele, A., Belachew, M., 2011. Surface wave tomography across Afar, Ethiopia: crustal structure at a rift triple-junction zone. Geophys. Res. Lett. 38, L24313. http://dx.doi.org/10.1029/2011GL046840.
Hofstetter, R., Beyth, M., 2003. The Afar Depression: interpretation of the 1960–2000 earthquakes. Geophys. J. Int. 155, 715–732.
Holland, T.J.B., Powell, R., 1998. An internally consistent thermodynamic data set for phases of petrological interest. J. Metamorph. Geol. 16, 309–343.
Ji, S., Zhao, P., Bia, X., 2003. Flow laws of multiphase materials and rocks from end-member flow laws. Tectonophysics 370, 129–145.
Kazmin, V., Shifferaw, A., Balcha, T., 1978. The Ethiopian basement: stratigraphy and possible manner of evolution. Int. J. Earth Sci. 67, 531–546.
Keir, D., Kendall, J.M., Ebinger, C.J., Stuart, G.W., 2005. Variations in late syn-rift melt alignment inferred from shear-wave splitting in crustal earthquakes beneath the Ethiopian rift. Geophys. Res. Lett. 32, L23308. http://dx.doi.org/10.1029/2005GL024150.
Keir, D., Ebinger, C.J., Stuart, G.W., Daly, E., Ayele, A., 2006. Strain accommodation by magmatism and faulting as rifting proceeds to breakup: seismicity of the northern Ethiopian rift. J. Geophys. Res. 111, B05314. http://dx.doi.org/10.1029/2005JB003748.
Kirstein, L., Peate, D.W., Hawkesworth, C.J., Turner, S.P., Harris, C., Mantovani, M.S.M., 2000. Early Cretaceous basaltic and rhyolitic magmatism in southern Uruguay associated with the opening of the South Atlantic. J. Petrol. 41, 1413–1438.
Kronenberg, A.K., Kirby, S.H., Pinkston, J., 1990. Basal slip and mechanical anisotropy of biotite. J. Geophys. Res. 95, 19257–19278.
Lavecchia, A., Clark, S.R., Beekman, F., Cloetingh, S., Burov, E., 2016. Thermal perturbation, mineral assemblages and rheology variations induced by dyke emplacement in the crust. Tectonics 35. http://dx.doi.org/10.1002/2016TC004125.
Logg, A., Mardal, K.A., Wells, G. (Eds.), 2012. Automated Solution of Differential Equations by the Finite Element Method. Springer, London, p. 723.
Luth, W.C., Jahns, R.I., Tuttle, O.F., 1964. The granite system at pressures of 4 to 10 kilobars. J. Geophys. Res. 69 (4), 759–773.
Mackenzie, G.D., Thybo, H., Maguire, P.K.H., 2005. Crustal velocity structure across the Main Ethiopian Rift: results from 2-dimensional wide-angle seismic modelling. Geophys. J. Int. 162, 994–1006.
Mahatsente, R., Jentzsch, G., Jahr, T., 1999. Crustal structure of the Main Ethiopian Rift from gravity data: 3-dimensional modeling. Tectonophysics 313, 363–382.
Menzies, M., Klemperer, S., Ebinger, C., Baker, J., 2002. Characteristics of volcanic rifted margins. In: Menzies, M., Klemperer, S., Ebinger, C., Baker, J. (Eds.), Volcanic Rifted Margins. Geol. Soc. Am. Spec. Paper 362, pp. 1–14.
Molly, E.W., 1959. Platinum deposits of Ethiopia. Econ. Geol. 54, 467–477.
Morley, C., 1988. Variable extension in Lake Tanganyika. Tectonics 7, 785–801.
Paterson, S.R., Fowler Jr., T.K., Schmidt, K.L., Yoshinobu, A.S., Yuan, E.S., Miller, R.B., 1998. Interpreting magmatic fabric patterns in plutons. Lithos 44, 53–82.
Patiño Douce, A.E., Johnston, A.D., 1991. Phase equilibria and melt productivity in the pelitic system: implications for the origin of peraluminous granitoids and aluminous granulites. Contrib. Mineral. Petrol. 107, 202–218.
Philpotts, A.R., Ague, J.J., 2009. Principles of Igneous and Metamorphic Petrology. Camb. Univ. Press, Cambridge,UK, p. 667.
Ranalli, G., 1995. Rheology of the Earth. Chapman and Hall, London, UK, p. 414.
Rooney, T., Furman, T., Bastow, I., Ayalew, D., Yirgu, G., 2007. Lithospheric modification during crustal extension in the Main Ethiopian Rift. J. Geophys. Res. 112, B10201. http://dx.doi.org/10.1029/2006JB004916.
Rosenberg, C.L., Handy, M.R., 2005. Experimental deformation of partially melted granite revisited: implications for the continental crust. J. Metamorph. Geol. 23, 19–28.
Shaw, H.R., 1965. Comments on viscosity, crystal settling, and convection in granitic magmas. Am. J. Sci. 263, 120–152.
Shelton, G., Tullis, J., 1981. Experimental flow laws for crustal rocks. EOS Trans. Am. Geophys. Union 62, 396.
Sibson, R.H., 1974. Frictional constraints on thrust, wrench and normal faults. Nature 249, 542–544.
Spear, F.S., 1993. Metamorphic Phase Equilibria and Pressure-Temperature-Time Paths. Mineral. Soc. Am., Washington D.C., p. 799.
Spear, F.S., Cheney, J.T., 1989. A petrogenetic grid for pelitic schists in the system SiO2-A1203-FeO-MgO-K20-H20. Contrib. Mineral. Petrol. 101, 149–164.
Thompson, R.N., Gibson, S.A., Dickin, A.P., 2001. Early Cretaceous basalt and picrite dykes of the southern Etendeka region, NW Namibia: windows into the role of the Tristan mantle plume in Paraná–Etendeka magmatism. J. Petrol. 42, 2049–2081.
Ukstins, I., Renne, P., Wolfenden, E., Baker, J., Ayalew, D., Menzies, M., 2002. Matching conjugate volcanic rifted margins: 40Ar/39Ar chronostratigraphy of pre- and syn-rift bimodal flood volcanism in Ethiopia and Yemen. Earth Planet. Sci. Lett. 198, 289–306. http://dx.doi.org/10.1016/S0012-821X(02)00525-3.
Vanderhaeghe, O., 2001. Melt segregation, pervasive melt migration and magma mobility in the continental crust: the structural record from pores to orogens. Phys. Chem. Earth A 26 (4–5), 213–223.
Vielzeuf, D., Holloway, J.R., 1988. Experimental determination of the fluid-absent melting relations in the pelitic system. Consequences for crustal differentiation. Contrib. Mineral. Petrol. 98, 257–276.
Wang, Z., Ji, S., 1999. Deformation of silicate garnets: brittle-ductile transition and its geological implications. Can. Mineral. 37, 525–541.
Whaler, K.A., Hautot, S., 2006. The electrical resistivity structure of the crust beneath the northern Main Ethiopian Rift. In: Yirgu, G., Ebinger, C.J., Maguire, P.K.H. (Eds.), The Afar Volcanic Province Within the East African Rift System. Geol. Soc. Lond. Spec. Publ. 259, pp. 293–305.
Wolfenden, E., Ebinger, C., Yirgu, G., Deino, A., Ayalew, D., 2004. Evolution of the northern Main Ethiopian rift: birth of a triple junction. Earth Planet. Sci. Lett. 224, 213–228.